



HAL
open science

Influence of hydration/dehydration on adsorbed molecules: Case of phthalate on goethite

R. Botella, ; Chiter, ; Costa, ; Nakashima, ; Lefèvre

► To cite this version:

R. Botella, ; Chiter, ; Costa, ; Nakashima, ; Lefèvre. Influence of hydration/dehydration on adsorbed molecules: Case of phthalate on goethite. *Colloids and Surfaces A: Physicochemical and Engineering Aspects*, 2021, 625, pp.126872. 10.1016/j.colsurfa.2021.126872 . hal-03379548

HAL Id: hal-03379548

<https://hal.science/hal-03379548>

Submitted on 15 Oct 2021

HAL is a multi-disciplinary open access archive for the deposit and dissemination of scientific research documents, whether they are published or not. The documents may come from teaching and research institutions in France or abroad, or from public or private research centers.

L'archive ouverte pluridisciplinaire **HAL**, est destinée au dépôt et à la diffusion de documents scientifiques de niveau recherche, publiés ou non, émanant des établissements d'enseignement et de recherche français ou étrangers, des laboratoires publics ou privés.

1 **Influence of hydration/dehydration on adsorbed molecules: Case of phthalate on goethite.**

2
3 Botella, R.^{1,2}; Chiter, F.¹; Costa, D.¹; Nakashima, S.^{2,3,4}; Lefèvre, G.^{1,*}

4
5 ¹ PSL Research University, Chimie ParisTech-CNRS, Institut de Recherche de Chimie Paris,
6 11 rue Pierre et Marie Curie, F-75005 Paris, France

7 ²Department of Earth and Space Science, Graduate School of Science, Osaka University,
8 Machikaneyama-cho 1-1, Toyonaka-shi, Osaka 560-0043, Japan

9 ³Research Institute for Natural Environment, Science and Technology (RINEST),
10 Tarumi-cho 3-6-32 Maison Esaka 1F, Suita-shi, Osaka 564-0062, Japan

11 ⁴Faculty of Environmental and Urban Engineering, Kansai University,
12 Yamate-cho 3-3-35, Suita-shi, Osaka 564-8680, Japan

13
14 * corresponding author: gregory.lefevre@chimieparistech.psl.eu

15
16
17
18 **Abstract:**

19
20 The behavior of adsorbed species on metal (hydr)oxides under water unsaturated conditions
21 has been seldom studied despite its major implications in several domains such as geochemistry and
22 heterogeneous catalysis. In this study, chemical forms of phthalate adsorbed on iron hydroxide
23 (goethite) were investigated by infrared spectroscopy upon hydration and dehydration of goethite
24 particle aggregates. Experimental results indicated important changes with relative humidity (RH) on
25 chemical forms of phthalates adsorbed on goethite. With increasing RH from the dried state, bidentate
26 phthalate surface complex is partially desorbed to form a protonated monodentate phthalate complex
27 by using protons from water molecules. This protonated monodentate phthalate is still kept adsorbed
28 on the goethite surface but becomes deprotonated at high RH values by solvating in liquid-like water
29 covering on the goethite surface. DFT calculations made on a simplified system support these
30 adsorption models. These results indicate that further studies are needed on the behavior of adsorbate
31 in water unsaturated systems including hydration/dehydration processes.

32
33 Keywords: phthalate, goethite, infrared, DFT calculations, hydration, dehydration, adsorption,
34 desorption

Introduction

Wetting/drying transitions are found in many systems both environmental [1] and surface and material chemistry [2, 3]. Thus, the speciation of adsorbates on several metal (hydr)oxides substrates has been studied for decades. For example, the solid/solution interfaces where the adsorption of different organic pollutants on iron hydroxides [4,5] and aluminum hydroxides [6,7] has been studied. At the interface solid/vapor or solid/gas, organic molecules can be used as acid-base probes [8,9], or in the context of catalysis, as reactive compounds [10,11].

Amongst the analytical methods to determine the speciation of adsorbates, infrared spectroscopy is the most versatile and was used extensively at both interfaces (solid/solution and solid/gas). In the case of organic molecules, this technique allows to identify the chemical groups in interaction with the surface [12], in the presence of a solvent like water, or at the solid/gas interface, and to estimate the strength of the interaction, and so, the geometry of the surface complex [13]. The interactions between carboxylic (carboxylate) groups and hydrated metal (hydr)oxides surfaces are especially well documented [14-19]. Adsorption is mainly ascertained by the study of symmetric and asymmetric stretching of the COO^- moieties (absorption bands around $1350\text{-}1450\text{ cm}^{-1}$ and $1500\text{-}1600\text{ cm}^{-1}$, respectively).

In the case of the study of wetting/drying transitions, infrared spectroscopy has the significant advantage to be able to probe the solvent (water) with a high sensitivity. Moreover, it allows to determine the environment of the water molecules and the structure of the phase. Thus, infrared analysis of water vapor on a surface has shown two kinds of water molecules: the first type is closer to the surface and is called ice-like water because of its spectral features reminding those of ice (stretching around 3200 cm^{-1}) [20, 21] but existing at ambient temperature, and another one more conventional “liquid-like” close to bulk water (stretching around 3400 cm^{-1}). Thus, these water species are indicators of the thickness of the water film at the surface and these characteristic bands of water allow to quantify, in an in situ and real-time manner, the wetting/drying evolution.

The drying of solids without adsorbate has been studied by infrared spectroscopy and has provided interesting results regarding the way water molecules organize themselves and their reactivity on a surface under unsaturated conditions [21, 22]. In the presence of dissolved species, several phenomena have been observed. For instance, the surface polymerization of silicic acid on ferrihydrite has been shown [23]. The impact of drying has also been studied for sulfate ions on iron (hydr)oxides [24-27], but without detailing the evolution of the surface speciation during the drying process (only the comparison between solid/solution and dried interfaces has been done). Other works have been performed on the drying behavior of diacids on both goethite [28] and clay minerals [29] with the same approach limited to the two different interfaces. In all those studies, infrared spectroscopy was the main technique to determine the speciation of the adsorbates. A solid/vapor system has also been investigated, focused on the gaseous formic acid adsorption on clays at decreasing relative humidity (RH) [30]. However, further studies are necessary by using more complex adsorbate including solid/water interfaces.

Few studies have been published on the effect of drying on the speciation of adsorbate, and even less on the behavior of these molecules while going through the different stages of hydration including the thin water film covering on the substrate [21]. Moreover, more rigid adsorbates, such as aromatic cycle containing phthalate molecule, have not been studied with respect to the change of relative humidity. Phthalates are soil pollutants [31,32] with chronic toxicity used as solvent, additives and plasticizers in daily life. It is also a simplified model compound representing chemical functionalities of natural organic matter (NOM) in aquatic and soil environments [33-35].

In this work, the behavior of the phthalate ions adsorbed onto goethite ($\alpha\text{-FeOOH}$), during a drying/wetting cycle has been investigated. Goethite has been chosen because it is a well-known model for soil adsorption with a good chemical stability. Infrared micro-spectroscopy was the main analytical technique, associated with a Quartz Crystal Microbalance (QCM). Moreover, to support interpretation of results observed at low relative humidity, DFT periodical calculations have been performed on the system to see the surface reaction evolution with the number of adsorbed water added one by one.

Materials and Methods

1. Goethite

Goethite samples were prepared after the methods of Schwertmann and Cornell [36] and Otsuka and Nakashima [37]. While they used $\text{Fe}(\text{NO}_3)_3$ and KOH in the methods, we used FeCl_3 and NaOH for avoiding remaining nitrate adsorbed on goethite surfaces and for possible future comparison with different ionic strength conditions.

100 mL of 0.1 mol.L^{-1} FeCl_3 solution and 180 mL of 5 mol.L^{-1} NaOH solution were mixed and diluted to 2 L with pure water (MilliQ: Electrical resistivity $> 18.2 \text{ M}\Omega \text{ cm}$). This suspension with rapid precipitation of brownish suspension was subdivided into two polypropylene vessels (1 L each) and incubated at $70 \text{ }^\circ\text{C}$ for 60 hours. Then yellowish-brown precipitates were filtered using $0.2 \text{ }\mu\text{m}$ Millipore filter. They were washed by pure water three times and dried in an electric oven at $50 \text{ }^\circ\text{C}$ for 4.5 hours.

The obtained precipitate was characterized by visible, Raman and infrared (IR) micro-spectroscopy, indicating that it was composed of goethite. X-ray diffraction pattern of the iron hydroxide showed six dominant peaks at $2\theta = 21,3^\circ, 26,4^\circ, 33,2^\circ, 34,7^\circ, 36,7^\circ, 39,2^\circ, 40,1^\circ$ and $41,3^\circ$, corresponding to reported peaks of goethite [36]. The BET surface area measured on a sample from another batch was $29.2 \text{ m}^2.\text{g}^{-1}$ [38] and its point of zero charge (PZC) is 8.6 by surface titration. Its surface charge at pH 6 was about $+0.04$ and $+0.05 \text{ mmol/g}$ for ionic strength of $I = 0.01$ and 0.1 , respectively. The morphology of goethite particles characterized by Laser Scanning Confocal Microscopy in a previous work showed that they are randomly oriented aggregates of a few hundred nm with some larger aggregates of a few micrometers [39].

2. Phthalate

Phthalic acid powder (Wako chemicals, 163-02462, Lot PKE1851) was dissolved in pure water to obtain 10 mL of 9.05 mM aqueous solution.

3. Phthalate-goethite suspension

In order to prepare phthalate adsorption on goethite, 1.125 g.L^{-1} of aqueous suspension of powdered goethite with 0.1 M NaCl was first prepared. Then $5.52 \text{ }\mu\text{L}$ of the phthalic acid solution (corresponding to 50 nmol) was added to 1 mL of the goethite aqueous suspension. The mixture was stirred during 24 hours by a magnetic stirrer to obtain adsorption equilibrium. Two duplicates were prepared: one for pH measurement and another for IR measurements. pH values were measured at the initial and final states during the 24 hours stirring: pH was initially 5.9 and after 24 hours stirring, it was 6.1. This pH value is close to natural water pH (between 6 and 8) and is expected to change upon dehydration procedure.

4. Relative Humidity Control System

For infrared (IR) measurements of phthalate-goethite mixtures during wetting/drying cycles, a plastic humidity control cell ($36 \times 36 \times 14 \text{ mm}$) with a CaF_2 window (20 mm diameter) was fabricated (Figure 1). The RH of the cell interior was controlled by flowing a mixture of dry air and water-saturated air with varying proportions. The dry air was provided from a dehumidifier (Jasco, AM-12) through a digital flow meter (KOFLOC, D8500). The water-saturated air was made by flowing the same dry air via another digital flow meter through two bottles of pure water (Milli-Q, Electrical resistivity $> 18.2 \text{ M}\Omega \text{ cm}$). The humidity and temperature in the cell were monitored every second by a small temperature and humidity sensor (SENSIRION, SHT 35 with a membrane filter) equipped with a data logger (Syscom, SCHM-1) connected to a PC with a USB cable. The humidity was increased from about 0.0 % to 78 % by changing the flow rates of humid and dry air by two flow meters at a total flow rate of about 1 L.min^{-1} .

144 **5. Quartz Crystal Microbalance**

145
146 In order to study effects of the wetting/drying cycle on phthalate-goethite mixtures, the
147 relative humidity control system combined with IR micro-spectroscopy and quartz crystal
148 microbalance developed by Kudo et al. [40,41] was used (Figure 1).

149 A QCM system (SEIKO EG&G, QCM922A) was used in this study for measuring weights of
150 adsorbed water on the phthalate-goethite mixtures placed on a gold electrode coating on an AT-cut
151 quartz of QCM sensor (SEIKO EG&G, QA-A9MAU(M)(SEP)) in a plastic container. Changes in
152 resonant frequency of quartz from the initial value (F_0) around 9.0 MHz were monitored at every
153 second when water was adsorbed under various relative humidity. These frequency changes can be
154 converted to mass changes for the present system [40,41].

155
156
157

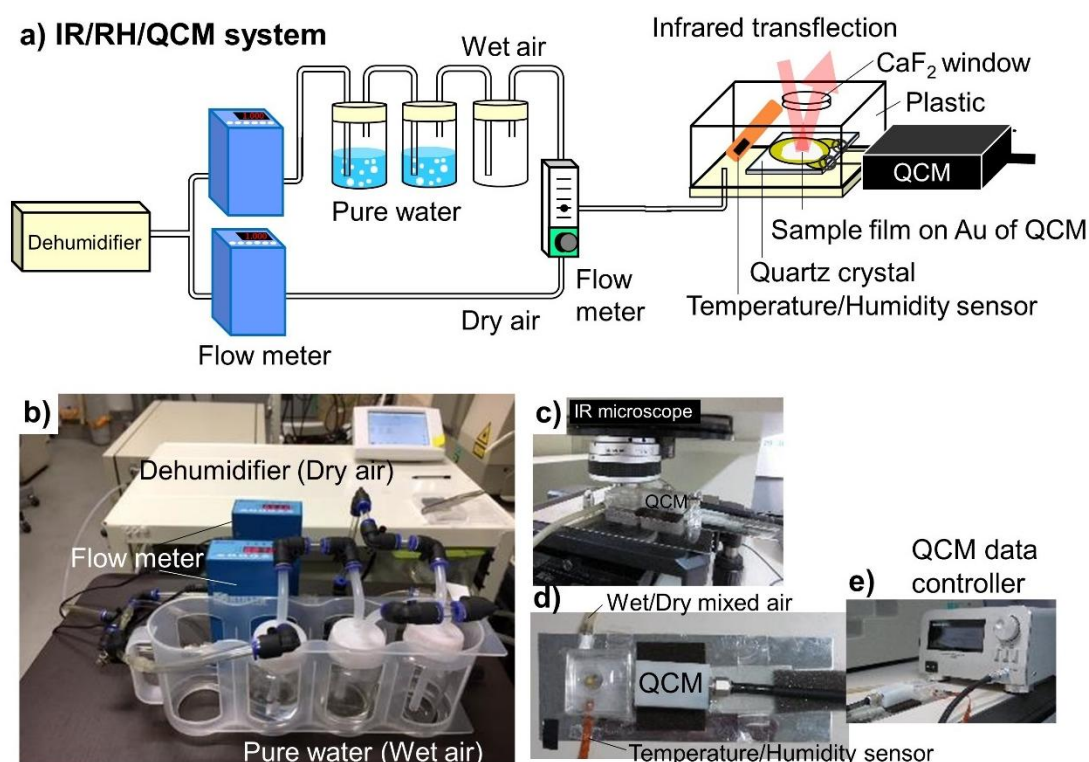


Figure 1. Infrared (IR) microspectroscopy combined with relative humidity (RH) control system and quartz crystal microbalance (QCM): (a) schematic image of the system, (b) photograph of the RH control system, (c) photograph of the RH control cell under an IR microscope, (d) close-up photograph of the RH control cell with QCM, and (e) QCM data controller.

158

159 **6. Preparation of phthalate-goethite particle aggregates**

160
161 One drop (5 μ L) of the phthalate-goethite mixture suspension was placed with a micropipette
162 on the Au electrode coating on an AT-cut quartz of the QCM in a plastic container (Figure 1). Dried
163 air was flowed in the plastic container with a flow rate of more than 1 L.min⁻¹ for about 30 to 45 min.
164 The dried phthalate-goethite deposit is expected to have a weight of about 5.625 μ g of goethite plus
165 about 7.4 ng of phthalate. As a reference, the goethite only system was also prepared, following the
166 procedure described above, using a suspension of goethite without phthalate.

167

168

169 **7. Infrared Microspectroscopy**

170

171 In order to evaluate changes in infrared (IR) spectra of the phthalate-goethite deposit, IR
172 transfection (transmission-reflection) spectra of the deposit on the Au electrode on QCM quartz

173 crystal were measured under different RH (0.0 – 77 %). The phthalate-goethite deposit on the QCM in
174 the plastic cell with a CaF₂ window was placed under a Fourier transform IR spectroscopy (FT-IR)
175 microscope (Jasco IRT30+FTIR680: a Cassegrain objective mirror with a magnification of 16, MCT
176 detector, ceramic IR source, and KBr beam splitter) (Figure 1). The environment outside the RH cell
177 was the ambient experimental room with normal air conditioning with the temperature around 28°C
178 and RH of about 60 %.

179 A background reflection spectrum was measured on the Au-coated quartz crystal without any
180 sample using an aperture size of 100 × 100 μm² and then a sample transfection spectrum was
181 measured on the deposit with the same aperture. All the spectra were obtained by accumulating 64
182 scans at a wavenumber resolution of 4 cm⁻¹. RH and temperature were monitored every second and
183 were averaged for 60 seconds, corresponding to the time needed to record the IR spectrum. These
184 transfection spectra were obtained in absorbance, and the band areas were measured after baseline
185 correction at each stable RH value. Every experiment was made in triplicate giving similar results.

186 8. Computational methods

187
188
189 The total energy calculations were performed within the density functional theory (DFT) and
190 the generalized gradient Pedrew-Burke-Erzenhoff (PBE) exchange correlation functional was used for
191 the whole study [42]. To solve the Kohn-Sham equations we use the Vienna Ab initio Simulation
192 Package (VASP version 5.4.1) [43,44]. VASP performs an iterative diagonalization of the Kohn-
193 Sham hamiltonian via unconstrained band-by-band minimization of the norm of the residual vector to
194 each eigenstate and via optimized charge density mixing routines. A smearing of 0.03 eV was used. In
195 the literature [45, 46, 47], cut-off of 500, 800 or 400 eV have been chosen. Because we wanted to
196 explore many configurations, we excluded the 800 eV cut-off. A test of convergence of energy with
197 the value of the cut-off was performed. We concluded that 400 eV was already a value where the
198 energy was converged. We used an energy cut-off of 400 eV for total energy calculations. The
199 electronic optimizations were done up to a convergence of 10⁻⁴ eV for the self-consistent loop and
200 until all forces on the atoms were lower than 0.02 eV.Å⁻¹ for the geometry relaxations.

201 Bulk goethite and its surfaces are routinely modelled with periodic density functional theory
202 (DFT)[47-49] including an on-site Coulomb repulsion term U (GGA + U) [46,50]. The (GGA + U)
203 was used in order to describe the strong correlation effects of the oxide. Several U values were
204 compared and the final values (H = 6, J = 1) were chosen to give the best agreement with the cell
205 parameters. For bulk FeOOH, the magnetic moment of the iron atoms was set at a starting point at the
206 experimental value, in the AFM order (++/-), and the optimized values were between 3.9 and 4.1, so
207 in agreement with experimental data and other theoretical calculations. The Van der Waals corrections
208 are calculated with DFT-D2 method of Grimme [50]. Furthermore, we applied dipole corrections
209 along the z axis, when calculating the adsorption energies (vide infra), since in our model the
210 adsorbate interacts only on one side of the slab.

211 Bulk goethite was considered in the Pbnm symmetry. The optimized cell parameters of bulk
212 goethite are 4.67×10.1×3.07 Å, in agreement with the experimental value of 4.63×9.96×3.02 Å [46]
213 and other theoretical works [46,47]. The K points grid was optimized and to model the bulk, a K
214 points grid (3x2x4) in the a, b and c directions, respectively, was used. The (001) surface contains four
215 layers. The three bottom layers were kept frozen. After the great number of configurations tested, the
216 calculations were performed at the Γ-point. Open shell calculations were performed. We found that the
217 Fe magnetic moments were between 3.9 and 4.1, whatever the Fe location (surface bulk) and the
218 nature of the ligand (phthalate or water). Surface goethite FeOOH (001) hydration/hydroxylation was
219 performed by saturating the surface iron atoms with 3 water molecules, thus recovering the bulk
220 octahedral Fe coordination. Although (001) facets are not the major surfaces exposed in goethite
221 nanoparticles, they are among the most reactive surface forming the most stable surface complexes.
222 The results on such a surface are expected to provide the existence of this mechanism on other facets.

223
224 We calculated the adsorption energy (ΔE_{ads}) according to the following equation:

$$225 \Delta E_{\text{ads}} = E_{\text{molecule+slab}} - E_{\text{molecule}} - E_{\text{slab}} \quad (1)$$

226
227

228 where $E_{molecule+slab}$ is the total energy of the optimized structure formed after the phthalate (or water)
 229 molecule is (chemically) absorbed on the goethite slab and $E_{molecule}$ and E_{slab} are the total energies of
 230 the non-interacting phthalic acid (or water) molecule and the slab, respectively. The adsorption of the
 231 molecule may be in the intact form, or in the dissociated form. In the latter case, one proton (for
 232 adsorbed water) or two protons (for adsorbed phthalate) are adsorbed on a vicinal surface O atom.

233 For the addition of n water molecules on the previously adsorbed phthalate ion, the adsorption
 234 energy is:

$$235 \Delta E_{addition} = E_{nH_2O+slab-phthalate} - n E_{H_2O} - E_{slab-phthalate} \quad (2)$$

236

237

238

239 Results

240

241 1. IR characterization of the goethite only system

242 For the goethite only system RH was changed from 0.0 up to 77 % and then down to 0.0%
 243 (Table 1). The RH value became stable within 15 minutes, so after keeping the same RH values for
 244 about 15 minutes it has been increased or decreased (Table 1).

245 Table 1. Time, temperature, relative humidity (RH), frequency shift (ΔF), mass changes (Δm), and total OH band area
 246 during wetting/drying processes of a goethite particle aggregates. “_” correspond to the points where the frequency shows a
 247 complex behavior.
 248
 249
 250

Time (min)	Temp (°C)	RH (%)	ΔF (Hz)	Δm (μg)	Total OH Band area
0	29.8	0.0	0	0	0.00
15	29.5	0.0	-120	0.13	0.03
30	29.4	9.8	-337	0.36	2.05
45	29.4	20.7	-385	0.42	4.12
60	29.3	30.4	-572	0.62	6.45
75	29.3	39.8	-701	0.76	7.68
90	29.2	49.3	-832	0.90	10.10
105	29.1	58.2	-923	1.00	15.61
120	29.1	67.8	2460	-2.67	27.21
135	29.0	74.9	_	_	92.06
150	29.0	75.3	_	_	91.54
165	29.1	74.5	_	_	86.00
180	29.0	77.3	_	_	293.89
195	29.0	74.1	131	-0.14	183.72
210	29.0	67.3	95	-0.10	41.84
225	29.0	59.8	131	-0.14	20.25
240	28.9	51.4	260	-0.28	15.65
255	28.9	43.1	368	-0.40	11.62
270	28.9	33.9	604	-0.65	7.93
285	29.0	24.6	380	-0.41	5.67
300	28.9	14.6	227	-0.25	4.08
315	28.7	1.9	0.61	0.00	0.91

251
 252
 253 Frequency values measured by QCM during RH changes on the deposits showed complex
 254 changes at higher RH values. Origins of these results will be discussed briefly below. Some of the
 255 results show an expected trend and will be quantitatively analyzed.

256
257
258
259
260
261
262
263
264

IR spectral changes with RH of the goethite only particle aggregates are shown in Figure 2 a) for wetting and Figure 2 b) for drying. The OH stretching of water molecules is visible in all the IR spectra during the wetting/drying processes by a broad band from 3600 to 3000 cm^{-1} with a peak around 3410 cm^{-1} (Figure 2 a), b)). A sharp band around 3123 cm^{-1} is due to OH stretching of Fe-OH species of goethite [53,54]. The 1640 cm^{-1} band is assigned to the bending vibration of H_2O molecules [54]. The peaks around 890 cm^{-1} and 792 cm^{-1} are assigned to bending (deformation) vibrations of Fe-O-H of goethite [53].

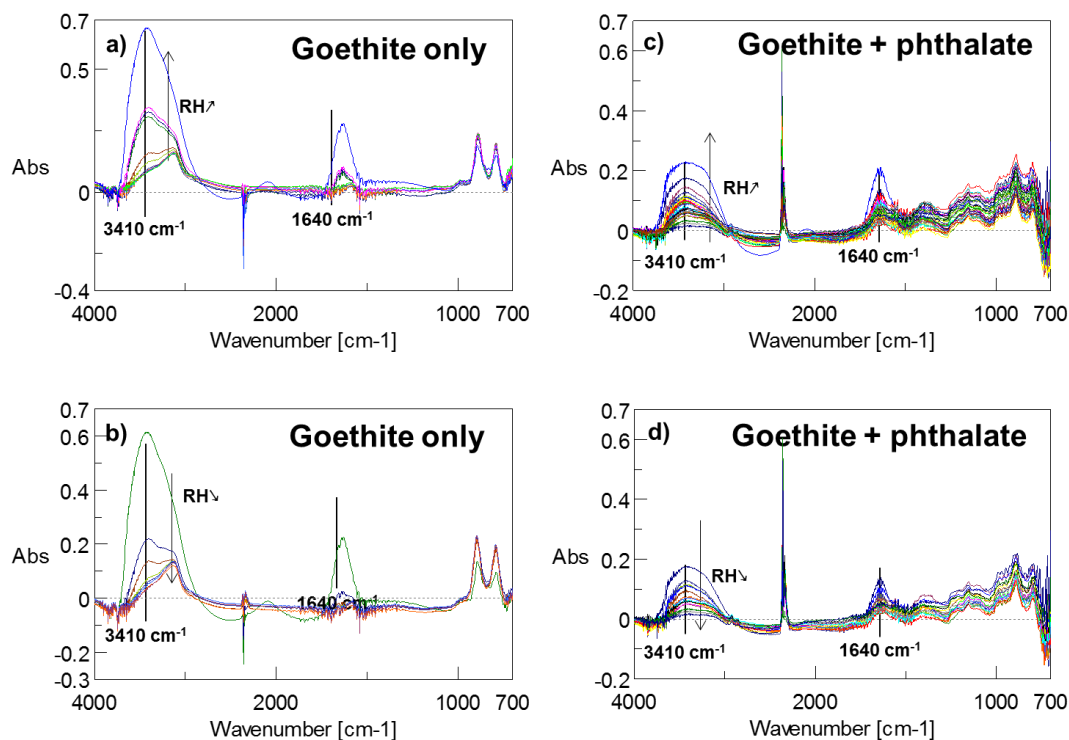


Figure 2: IR spectral changes with relative humidity (RH: %) of the goethite only system during (a) wetting and (b) drying processes. c) and d) are for a phthalate sorbed goethite system during (c) wetting and (d) drying processes.

265
266
267
268
269
270
271
272
273
274
275
276

In Figure 3 a), the OH stretching band area of the goethite particle aggregates with a linear baseline from 3730 to 2995 cm^{-1} is plotted against RH. During the wetting process, a slight increase with RH is observed for low RH values, then a sharper increase above 60 %. A similar trend is found during the drying process. In Figure 4 a), the Fe-O-H band areas around 890 cm^{-1} (950-830 cm^{-1}) during the wetting and drying processes are plotted against RH. The value is relatively constant at low RHs and decreases greatly at RH higher than 60%. The Fe-O-H band area follows a similar trend for drying process, without hysteresis.

2. IR spectral changes for goethite + phthalate system

IR spectral changes with RH of the goethite + phthalate deposit are shown in Figure 2 c) for wetting and Figure 2 d) for drying. The sharp band at 3123 cm^{-1} due to OH stretching of Fe-OH species of goethite is not clearly observed in the goethite + phthalate system because of the strong overlap with a band around 3000 cm^{-1} probably coming from non-adsorbed or partially adsorbed phthalic acid molecules. The broad band in the 3600 – 3000 cm^{-1} region and the 1640 cm^{-1} band is overlapped with bands of phthalate/phthalic acid molecules. The peaks around 890 cm^{-1} and 792 cm^{-1} due to bending (deformation) of Fe-O-H of goethite are less visible than in the goethite only system.

284 The OH stretching band areas were measured with a linear baseline from 3730 to 2995 cm^{-1}
 285 for the goethite + phthalate deposit during the wetting and drying processes and were plotted against
 286 RH in Figure 3 b) (Table 2). This wavenumber region may include contributions from OH of goethite
 287 (FeOOH) and phthalate (COOH). The OH bands of goethite around 3125 cm^{-1} are principally kept
 288 unchanged, with some minor changes of surface OH species hydrogen-bonded to water molecules.
 289 Band area for the signal at around 1640 cm^{-1} has been monitored as well and showed a similar trend to
 290 the OH stretching band in Figure 3. The same position of the goethite particle aggregates on the gold-
 291 coated quartz crystal has been monitored throughout the entire experiment. As a consequence, any
 292 spectral change observed is attributed to water adsorption/desorption. As observed in the goethite only
 293 experiments, the OH stretching band of goethite + phthalate deposit first increased slightly with RH
 294 and greatly from 60 % during the wetting process. The OH band follows the similar trend during the
 295 drying process but showing with a small hysteresis loop between RH = 60 – 80 % (Figure 3 b)). If
 296 compared to the goethite only system, the maximum band area is smaller.

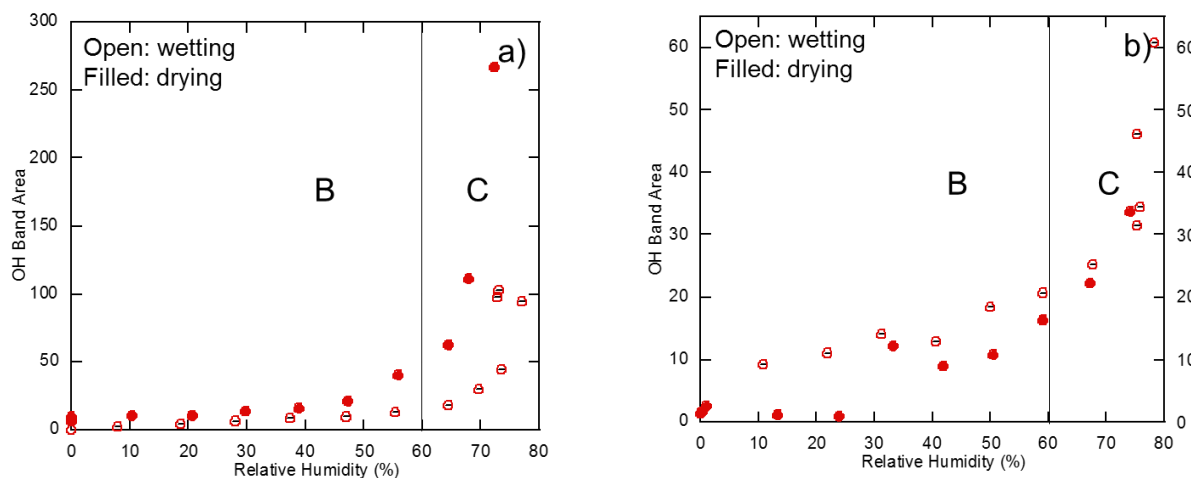


Figure 3: OH stretching band area as a function of relative humidity for a) goethite only and b) phthalate-adsorbed goethite. Open circles correspond to the wetting branch and closed circles to the drying branch. Vertical lines are guides to see the transitions between regions B and C mentioned in the literature [21], the region A is difficult to isolate.

297
 298
 299 Table 2. Time, temperature, relative humidity (RH), frequency shift (ΔF), mass changes (Δm) and total OH band area during
 300 wetting process of a goethite particle aggregates after adsorption of phthalates.”_” correspond to the points where the
 301 frequency shows complex behavior.

Time (min)	Temp (°C)	RH (%)	ΔF (Hz)	Δm (μg)	Total OH Band area
0	29.0	0	0	0	17.4
15	29.0	6.6	-21	0.02	21.32
30	28.9	17.5	-140	0.15	25.53
45	28.8	27.3	-132	0.14	27.66
60	28.8	36.5	–	–	29.23
75	28.8	45.9	–	–	31.53
90	28.7	53.1	–	–	32.85
105	28.6	60.1	–	–	36.65
120	28.6	68.3	-219	0.24	46.68
135	28.7	75.6	1253	-1.36	57.26
150	28.6	75.6	-46	0.05	48.28
165	28.6	75.3	-1257	1.36	51.24
180	28.6	78.1	-3677	3.98	81.93
195	28.6	73.9	3802	-4.12	40.62
210	28.5	66.7	–	–	34.00
225	28.5	58.9	–	–	28.97
240	28.5	50.5	–	–	25.67
255	28.4	42.1	–	–	26.55
270	28.5	33.2	-194	0.21	21.76
285	28.4	24.7	298	-0.32	14.91
300	28.4	13.9	284	-0.31	15.81
312	28.4	2.3	214	-0.23	14.62

303

304 The Fe-O-H band areas around 890 cm^{-1} ($950\text{-}830\text{ cm}^{-1}$) of the goethite + phthalate deposit
 305 during the wetting and drying processes were plotted against RH (Figure 4 b)). During wetting, it
 306 increases quasi-linearly at low RHs ($<30\%$), remains relatively constant at $\text{RH} = 30\text{-}60\%$ and decreases
 307 at RH higher than 60% . The band area does not show a similar trend for drying process: first the band
 308 increases greatly, then a decrease is observed around 30% relative humidity.

309

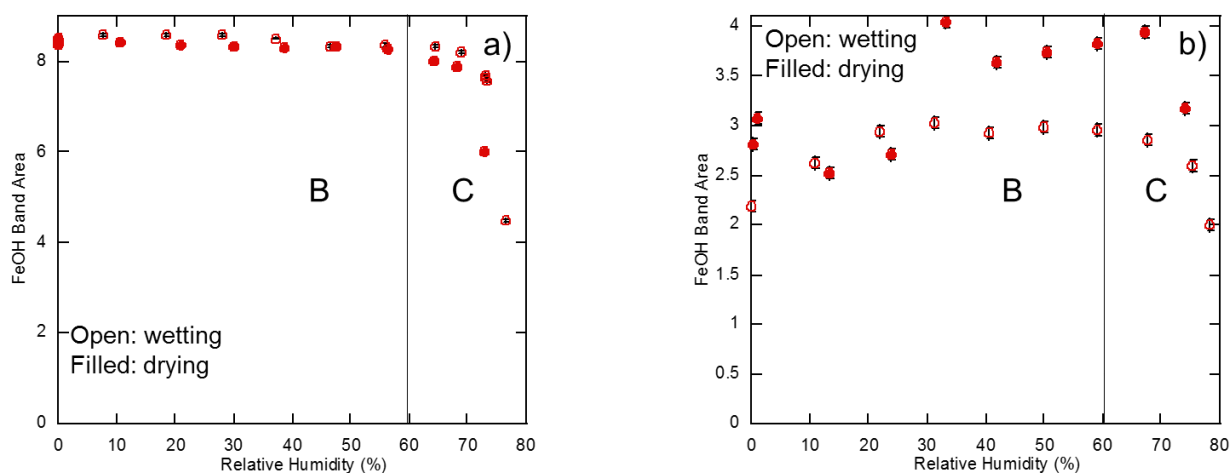


Figure 4: Fe-O-H bending band areas as a function of relative humidity for a) goethite only and b) phthalate adsorbed goethite. Open circles correspond to the wetting branch and closed circles to the drying branch. Vertical lines are guides to see the transitions between regions B and C mentioned in the literature [21].

310
311
312
313
314
315
316
317
318
319
320
321
322
323
324
325
326
327
328
329
330
331
332
333
334
335
336
337
338
339
340
341
342
343
344
345
346
347
348
349
350
351
352
353

Discussion

1. Amounts of water adsorbed to the goethite particle aggregates with and without phthalate

Quartz Crystal Microbalance (QCM) data on frequency changes of the QCM sensor during wetting/drying cycles of goethite (+phthalate) deposits gave complex changes with RH at higher RHs (figures not shown). At low RHs (RH < 50%), QCM frequencies decreased with RH with some fluctuations. Between RHs of 50 to 75 %, frequencies showed complex fluctuations with RH. These changes can be related to viscoelastic perturbations due to adsorption of multiple water molecular layers and structural modification of aggregates of goethite nanoparticles. As RH is raising, small menisci may appear between the grains of goethite (and especially at contact points between the grains at first), applying some hydrostatic pressure on the solid particles. As a result, the forces applied may be responsible for small displacements of the grains with respect to their resting (dry) state. Moreover, the formation of menisci is associated with the appearance of a liquid phase between the grains. It is possible that electric charge is building up on the surface that is producing some small rearrangements of the deposit, impairing the oscillations of the QCM device [54]. The deposit is contacting the gold surface of the QCM plate and the small displacements of the grains may change the oscillating frequency of the plate and eventually change the resulting current, producing some important changes in the measurements. At RH of about 75 % to 78 %, QCM frequencies decreased greatly, in agreement with the significant increase of OH band areas (Figure 3).

The final values of ΔF (Hz) during each RH step for RH = 0 – 50 % and 78 % can be converted to mass changes Δm (μg) (Table 2). In Figures 5 and 6, they have been plotted against the total OH band areas (shown in Figure 3). For the goethite only system, OH band area shows a quasi-linear trend with the cumulated mass change area from 0 to around 1.5 μg (Figure 5 a)), while the goethite + phthalate system shows a different trend with the cumulated mass change (Figure 6 a)), resulting in a strong hysteresis phenomenon. Such measurements reflect the evolution of the integrated molar absorption coefficient with the change of surface hydration state. The differences between Figure 5 and Figure 6 shine a light on the difference of interaction of water vapor with goethite surface after adsorption of phthalate. However, such changes should be interpreted with caution as they correspond to an average of the many OH species present in the system. The water mass measurements by QCM are not converted to numbers of water layers, because high levels of approximation are necessary. We prefer to stay on a monolayer/multilayer picture of the surface hydration.

For more quantitative comparison, the OH band areas should be normalized by some band areas characteristic of the solid. Although the Fe-O-H band area showed unexpected changes for the goethite + phthalate system (Figure 4 b)), it is the most representative band of goethite. Therefore, the normalized OH band areas were divided by the Fe-O-H band areas and are plotted against RH in Figure 7. The use of the normalization enables to confirm the changes of the OH band area with respect to the amount of solid. The presence of phthalate molecules adsorbed on the goethite surface results in a hysteresis loop on the OH band area.

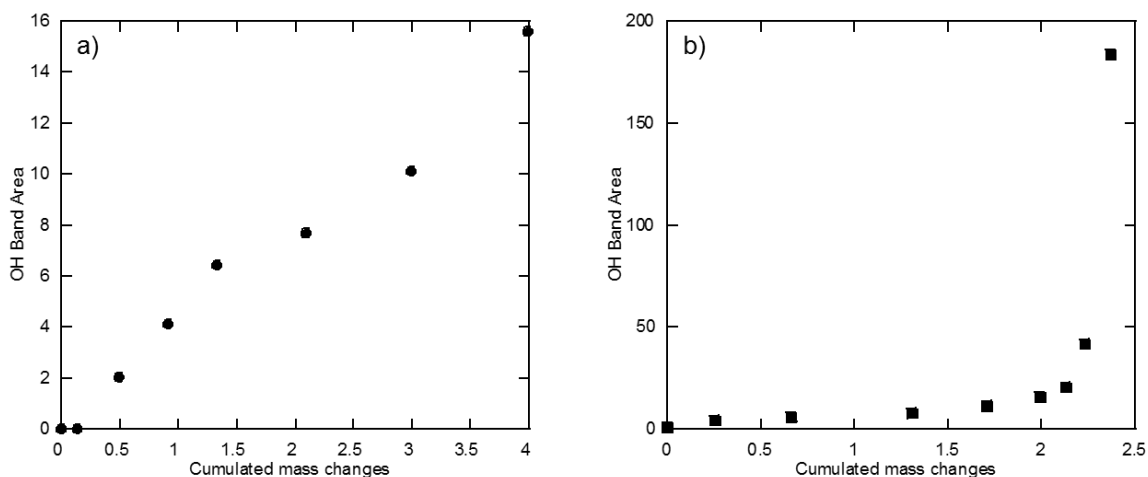


Figure 5: OH stretching band areas as a function of cumulated mass changes of a goethite film for the a) wetting branch and b) drying branch.

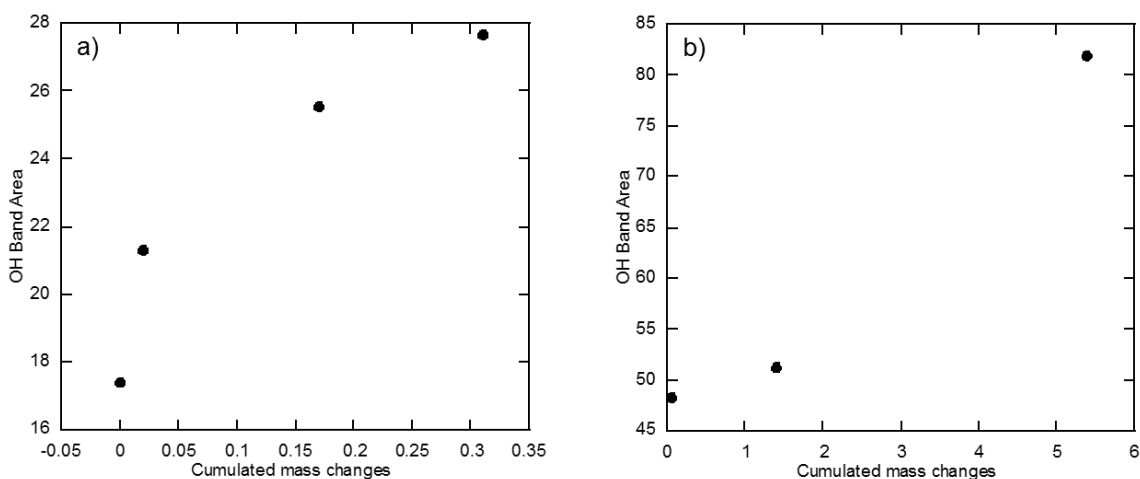


Figure 6: OH stretching band areas as a function of cumulated mass changes of a phthalate adsorbed goethite particle aggregates for the a) wetting branch and b) drying branch.

354
 355
 356
 357
 358
 359
 360
 361
 362
 363
 364
 365

Weight ratios of adsorbed water to goethite particle aggregates are about 3.6 times larger for the goethite only system than the goethite + phthalate system at about RH = 78% (Tables 1 and 2). On the other hand, the normalized OH band area are about 1.6 larger for the goethite only system than the goethite + phthalate system at about RH = 78% (Figure 7). It should be noted that this factor can be considered as a minimum value, since the surface Fe-O-H bands can be decreased by the adsorbed phthalates on the goethite surface. Thus, the presence of phthalate on the goethite particle aggregates was found to decrease greatly the adsorption behavior of water both from the QCM data and the infrared OH bands.

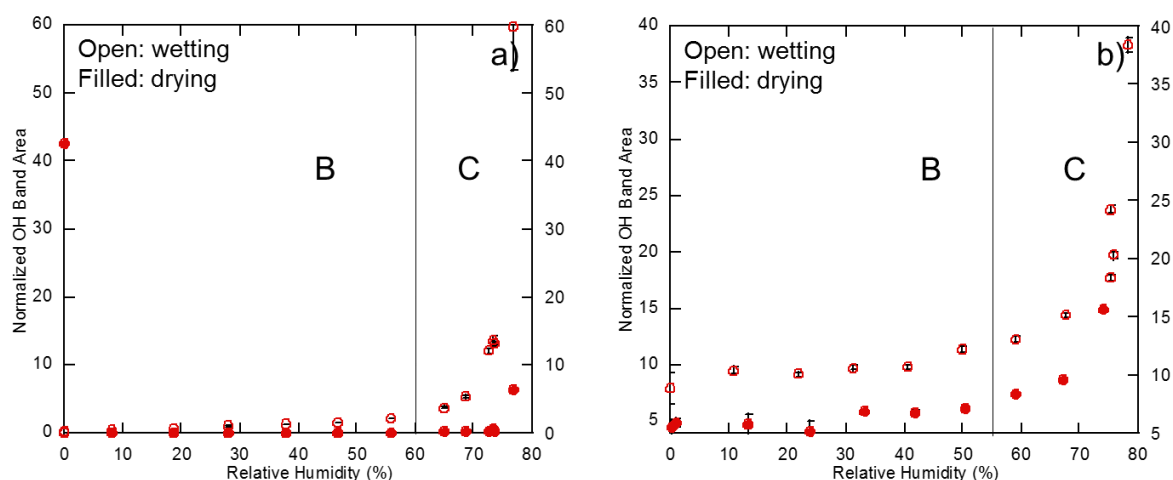


Figure 7: Normalized OH stretching band areas (divided by Fe-O-H band areas) as a function of relative humidity for a) goethite only and b) phthalate adsorbed goethite. Open circles correspond to the wetting branch and closed circles to the drying branch. Vertical lines are guides to see the transitions between regions B and C mentioned in the literature [21].

367
368
369

2. Water adsorption isotherms

370 Before examining phthalate bands, we will first discuss shapes of the water adsorption
371 isotherms of the goethite only and goethite + phthalate systems. Since adsorbed water masses could
372 not be obtained for all the RH range, the normalized OH band areas will be used for representing
373 adsorption isotherms (Figure 7). These can be discussed in terms of three regions based on some
374 typical literatures for adsorption isotherms [57, 21]: region A; monolayer adsorption of ice-like water
375 molecules, region B; multilayer adsorption of various water molecules, region C; capillary
376 condensation of liquid-like water. Ice-like water corresponds to water molecules strongly interacting
377 with the surface via short hydrogen bonding. This strong interaction is very likely to impair the
378 mobility of these water molecules at the surface and therefore limit any transport in this relative
379 humidity region. On the other hand, C region is mainly composed of liquid-like water molecules
380 whose properties (such as mobility) are close to those of liquid water. Transport phenomena are
381 assumed to be favored in this region. B region is a transition region and exhibit a mixture of the
382 respective behaviors of A and C.

383 For the goethite only system, the adsorption isotherm appears to have S shape with region A
384 possibly between $RH = 0 - 30\%$ based on a literature [21] with only minor amounts of adsorbed water.
385 Based on the surface of deposited goethite and the adsorbed water mass, the thickness of the water can
386 be estimated to 0.84 nm for 8.1 %RH. For the region B, the water mass is unknown, and this
387 calculation cannot be made. For the region C, the thicknesses of water layers can be more than 6.5 nm
388 (ca 67.8 %RH, see Table 1), which is consistent with the thickness threshold for the liquid-like
389 expected behavior. For the goethite + phthalate system, the adsorption isotherm has also a S shape
390 with region B for $RH = 30 - 55\%$ and region C above 55 %, rather similar to the goethite only system.
391 Region A is difficult to isolate. Due to the fact that the sample is composed of particle aggregates
392 instead of a flat surface as studied in the literature [21], it has been difficult to interpret the data in
393 terms of numbers of water layers (one, two...). For this reason, only the region A (mono to few-layers)
394 and region C (multilayers) are considered. It could result from the low surface area ($S_{BET} = 29.2 \text{ m}^2 \cdot \text{g}^{-1}$)
395 of the goethite used and therefore the expected increase of the band area of the A region is difficult
396 to be observed.

397
398
399

3. Phthalate Bands (COOH)

400 A magnification of the IR spectra focused on phthalate/phthalic acid molecules are shown in
401 the supporting information part (Figures S1 and S2). An IR band in the $3000 - 2830 \text{ cm}^{-1}$ region

402 results from the combinations of fundamental bands of COOH groups of fully or partially protonated
 403 phthalic acid [59]. Due to its smaller bandwidth with respect to the other wide signals ($3730\text{-}2995\text{ cm}^{-1}$)
 404 ¹), this band is always observed throughout the hydration/dehydration cycle. Moreover, they are
 405 isolated, which is not the case in the $1770\text{ - }1300\text{ cm}^{-1}$ wavenumber range, characteristic of the
 406 carboxylic acid/carboxylate signals. The band area is plotted vs. time in Figure 8a. The COOH
 407 combination band area increases gradually from RH = 0 to 76 % but drops around the highest RH =
 408 78 %. Upon the start of dehydration step, the $3000\text{ - }2830\text{ cm}^{-1}$ band increases and returns to its value
 409 at ca 76 RH%. A partially reversed trend with some fluctuations is observed during the drying process.
 410 Results can be displayed in the form of an isotherm in Figure 8 b), where the same trend as Figure 8 a)
 411 as a function of RH can be observed.

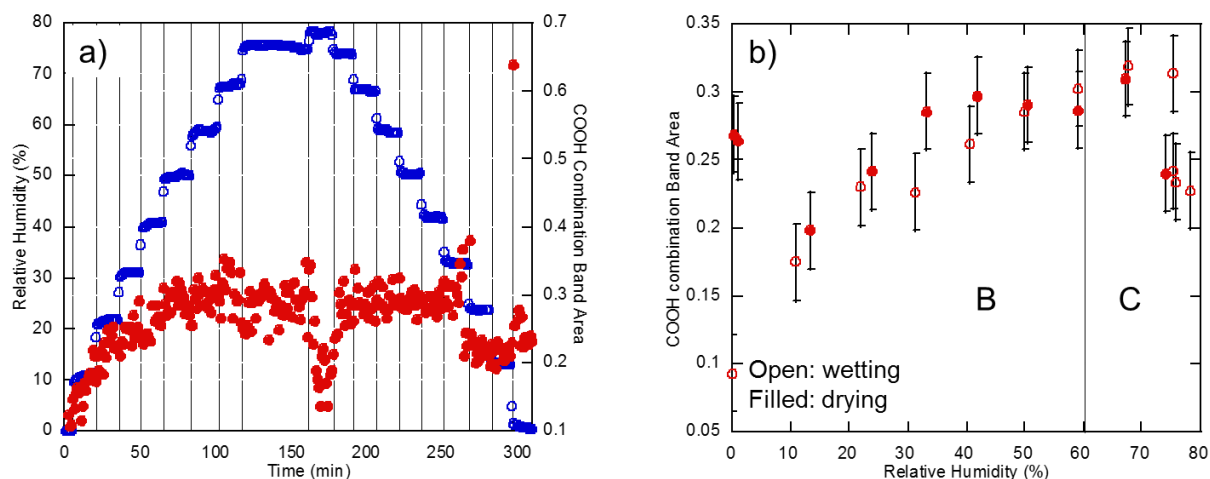


Figure 8: a) Evolution of the COOH combination band area (red filled circles) and relative humidity (blue open circles) as a function of time. Vertical lines are separating the increases and decreases of RH. b) Evolution of the COOH combination band area as a function of relative humidity. Open circles correspond to the wetting branch and filled circles to the drying branch. The vertical line is a guide to see the transition between regions B and C.

412
 413 It should be noted that the COOH band does not follow the RH change steps but shows
 414 somewhat a gradual change. This is very surprising, since even if the change is related to kinetics of
 415 the evolution of the COOH group, it should at least be influenced by the increase of the thickness of
 416 the water film on the solid surface. A possible explanation would be the relation between the increase
 417 of COOH band and the protonation of COO^- groups of phthalate adsorbed on the positively charged
 418 goethite surface. Indeed, the molecular water adsorbed at the goethite surface might dissociate to
 419 provide protons to form carboxylic acid. The resulting OH^- would react with the protonated surface
 420 groups of goethite to give Fe-O-H species. In fact, the Fe-O-H band area shows similar kinetic
 421 behavior to the COOH bands, supporting such a mechanism (Figure 9).

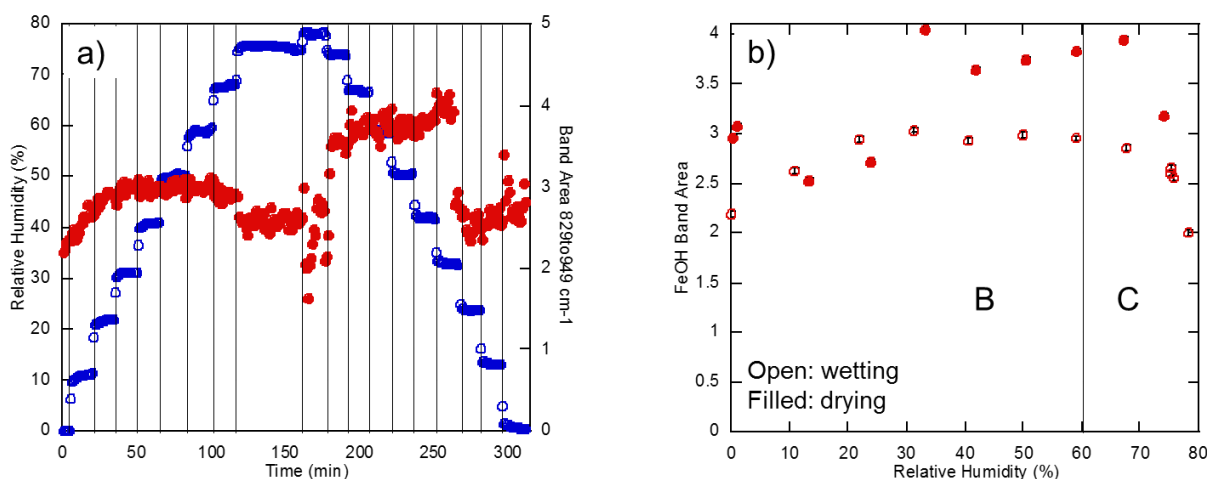


Figure 9: a) Evolution of the FeOH bending band area (red filled circles) and relative humidity (blue open circles) as a function of time. Vertical lines are separating the increases and decreases of RH. b) Evolution of the FeOH bending band area as a function of relative humidity. Open circles correspond to the wetting branch and filled circles to the drying branch. The vertical line is a guide to see the transition between regions B and C based on the literature [21].

422 The sudden decrease of the COOH band at RH > 76% corresponds to the region C with the
 423 presence of liquid-like water. In these conditions, the system is closer to the solid/solution equilibrium,
 424 dominated by the adsorption of carboxylate ions. Therefore, this decrease can be explained by the
 425 deprotonation of RCOOH, which results in a lower concentration of carboxylic groups.

4. Phthalate Bands (CO)

426
 427
 428 IR bands in the 1130 – 1191 cm⁻¹ region are considered to be due to stretching of CO groups
 429 of phthalate [59]. The CO band areas are plotted against time together with RH values (Figure 10 a)).
 430 The CO band area increase gradually with time from RH = 0 to 76 % but decreased greatly around the
 431 highest RH = 78 %. As observed in the analysis of the COOH phthalate bands, a complete reversibility
 432 of the decrease of the CO band upon the start of the dehydration procedure is observed. For the rest of
 433 the dehydration process, band area showed a reverse trend with some fluctuations during the drying
 434 process (Figure 10 a)).
 435

436 The trend of this CO band is very similar to the one of the COOH band (Figure 8 a)). This
 437 increase of CO stretching band confirms the protonation of COO⁻ groups of phthalate adsorbed at the
 438 goethite surface. The inverse changes of the CO band area together with that of the COOH band
 439 around RH = 78% (Figure 8 a), Figure 10 a)) can be interpreted as the deprotonation of the phthalic
 440 acid in contact with bulk water at pH higher than its pK_a.

441

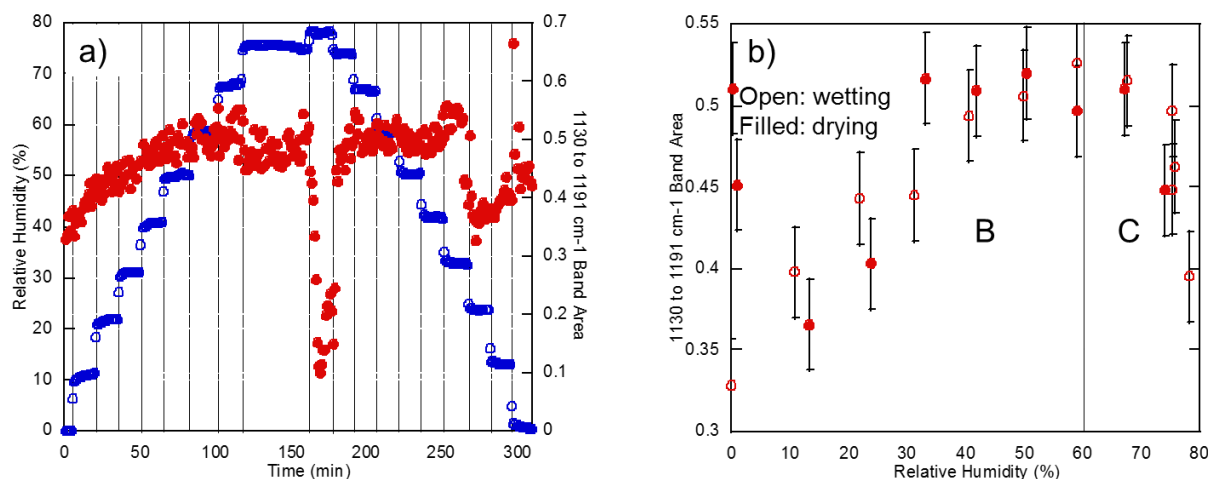


Figure 10: a) Evolution of the CO stretching band area (red filled circles) and relative humidity (blue open circles) as a function of time. Vertical lines are separating the increases and decreases of RH. b) Evolution of the CO stretching band area as a function of relative humidity. Open circles correspond to the wetting branch and filled circles to the drying branch. The vertical line is a guide to see the transition between regions B and C based on the literature [21], but region A is difficult to isolate.

442
 443
 444
 445
 446
 447
 448
 449
 450
 451
 452
 453
 454
 455
 456
 457
 458
 459
 460
 461
 462
 463
 464
 465
 466
 467
 468
 469
 470
 471
 472
 473
 474
 475
 476
 477
 478
 479
 480
 481
 482
 483
 484
 485
 486
 487
 488
 489
 490
 491
 492
 493
 494
 495

5. Phthalate adsorption model

Based on the above results and discussion, the following model for phthalate behavior during its adsorption on goethite can be proposed.

The phthalate species are considered to be adsorbed on the goethite surface during the 24 hours stirring of the mixture with a surface coverage of $0.8 \mu\text{mol.m}^{-2}$, mainly in the form of inner sphere complex both in the monodentate and the bidentate forms [59]. After dehydration of the suspension on the QCM plate, surface density of phthalate is expected to be $1.6 \mu\text{mol.m}^{-2}$. Under optical microscope, NaCl crystals have been observed in the dried phthalate-goethite particle aggregates on the QCM sensor. Although no elemental analysis has been performed on the crystals, the fact that the same images are observed during the experiment on goethite alone tends to confirm their chemical identity. Moreover, NaCl was a thousand time more concentrated than phthalic acid in the suspension, thus NaCl reaches its solubility limit long before sodium phthalate does. While NaCl crystallization is starting, the concentration of Na^+ and Cl^- is above the solubility limit (ca 6 M) and is impairing both outer-sphere and inner sphere complex formation [56]. Therefore, the subsequent water evaporation leads to the precipitation of NaCl, and sodium phthalate remains under-saturated, allowing the adsorption of phthalate species. Even though sodium phthalate is not expected to precipitate, by-products of the drying phenomenon could be solvated ion pairs with Na^+ ions or the surface (i.e. outer sphere complexes).

One way to understand these experimental observations is the following model: with increasing RH, water is going to substitute part of the phthalate molecules adsorbed on the goethite surface, forming partially desorbed and therefore unstable carboxylate moiety such as the following reaction scheme:



$\phi_{\text{COO}}^{\text{COO}}$ designates the phthalate molecule with adsorbed (COO) moiety and free (COO^-) moiety. From this reaction scheme, the initial state is assumed to be a physically sorbed bidentate surface complex, which is implied by the existence of the reversibility of the C region (ca 78%RH). The chemical sorption of phthalate molecules can occur either as a monodentate or a bidentate configuration. The hydration of the surface can induce a protonation and desorption of a carboxylate group of the adsorbate. If the monodentate surface complex is protonated, it becomes an outer-sphere complex free to diffuse outside of the IR spot at high relative humidity. As a complete reversibility of the COOH and CO band areas is observed between hydration and dehydration cycles, such expected transport did not take place. This can be explained by the fact that the phthalate molecule are still anchored to the surface by another COO. Thus, this surface reaction is leaving one COO^- still bound to goethite surface. This type of behavior has been noticed in another work studying the behavior of formic acid in water unsaturated atmosphere [10]. Although water can solvate carboxylate groups in aqueous solution, the thin water film is preventing to have solvation shell stabilizing the COO^- group newly formed, and a chemisorbed surface water could deprotonate and trigger a proton transfer to form a carboxylic acid group that is able to fit in the hydrogen bond network of the surface. This would result in the formation of new hydroxyl groups parallel to the protonation of carboxylic acid.



By the formation of a carboxylic group, a band at 1700 cm^{-1} (C=O stretching) would be expected to appear, but could not be recognized in the spectra. Interaction of the COOH with surface-bonded ice-like water could red-shift this C=O band overlapping with COO^- and H-O-H bands around 1600 cm^{-1} . Strong hydrogen bonding, such as in carboxylic acids for example, has been known to shift IR bands of carboxylic acids tremendously (around 100 cm^{-1}) [60]. Strong hydrogen bonding is also

496 found at the surface of metal oxide at low relative humidity, thanks to the ice-like water molecules and
 497 would explain why typical signals of COOH moieties are not observed in the spectra. Such a trend is
 498 confirmed by the DFT calculations.

499
 500 At highest RHs with capillary condensation of liquid-like water, the acid-base equilibrium of
 501 carboxylate group at $\text{pH} > \text{pKa}$ could take place to deprotonate COOH forming hydronium ion H_3O^+ :
 502



503
 504 Since the partially deprotonated phthalates are still confined to the surface, they will be
 505 returned back to dimer upon drying of liquid-like water.
 506

507
 508 In order to confirm the above interpretation, DFT calculations have been performed. The
 509 calculations are detailed in the materials and methods section. After finding the most stable phthalate
 510 molecule on the (001) facet, which is a binuclear adsorption mode, more stable by 0.6 eV than the
 511 mononuclear one, we gradually completed the coordination sphere of the surface Fe atoms. In total, 25
 512 configurations were studied, where the positions of the water molecules were changed in order to
 513 reach the best local minimum. More adsorbed water molecules warrant more configurations tested per
 514 model. Again, the scope of the study was not to perform an exhaustive study of the potential energy
 515 surface, but rather to compare, at a given water coverage, and in a given water configuration, the
 516 mono- versus binuclear configurations of phthalate adsorption. The binuclear configuration is
 517 compared to the configuration with the same amount of water molecules adsorbed, but in which the
 518 phthalate adsorption mode is mononuclear. The schematic view in Figure 11 aims at helping to
 519 understand how the phthalate molecule is interacting with the surface, as well as the fate of the vicinal
 520 Fe sites. the site “Fe 1” is the site accepting the COO moiety in a bidentate adsorption mode. The sites
 521 “Fe 3” and “Fe 4” are saturated with two adsorbed water molecules. The site “Fe 2” receives either the
 522 COOH adduct, the COOH adduct and one water molecule, or two water molecules. When phthalate is
 523 adsorbed only on “Fe 1”, the adsorption is mononuclear. When phthalate is co-adsorbed on “Fe 1” and
 524 “Fe 2”, the adsorption is binuclear.
 525

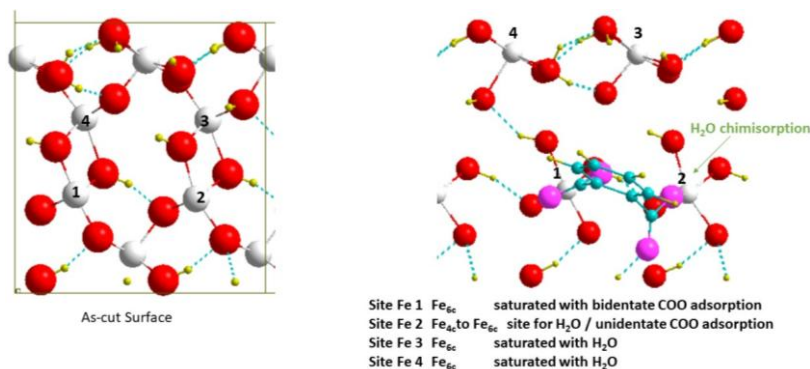


Figure 11: Schematic views from above :a) pristine (001) surface a) and b) with phthalate adsorbed on the goethite surface (001) surfaces.

526
 527 For example, the bidentate (Bi) configuration (Bi, 1,0), in which “Fe 2” coordination is
 528 saturated, is compared to the monodentate (Mono) configuration with the same water loading, (Mono,
 529 1,0) in which “Fe 2” is 5 fold coordinated. Note that in the mononuclear configuration, a surface
 530 proton is transferred to the desorbed COO to stabilize the COOH moiety. This re-protonation of COO
 531 was indeed observed experimentally in the present work (see above).
 532

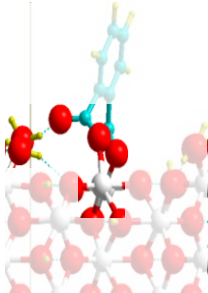
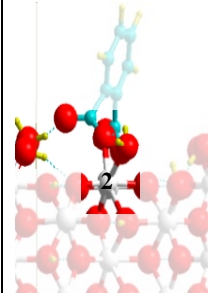
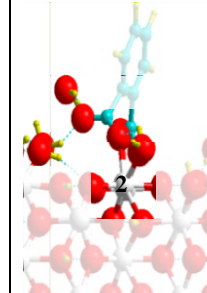
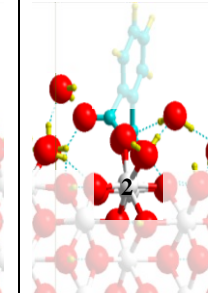
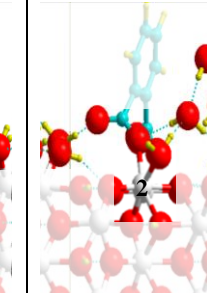
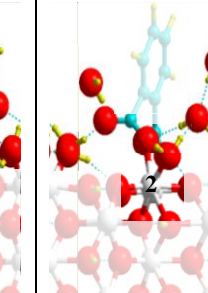
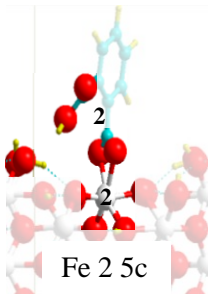
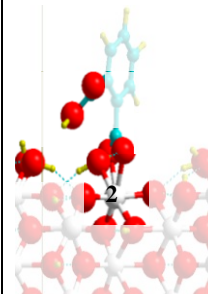
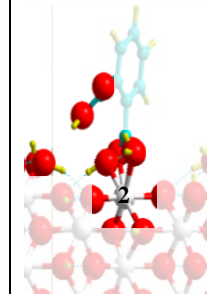
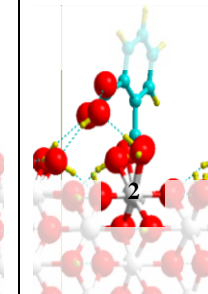
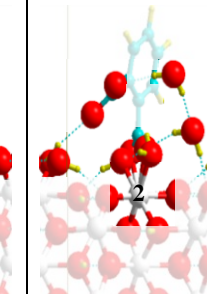
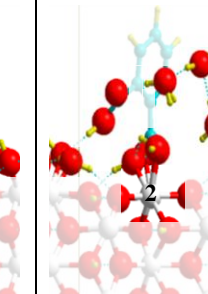
533 The most stable configurations obtained are reported in Table 3. For each water coverage,
 534 both configurations, mononuclear and binuclear are reported, together with the difference in energy
 535 between these configurations. It clearly appears that, at low water loading (4 water molecules adsorbed
 536 on iron atoms, coverage $4.2 \text{ molecule/nm}^2$), the binuclear configuration is more stable by 0.61 eV than
 537 the mononuclear one, which is explained by the fact that the surface iron “Fe 2” has not its full
 538 coordination sphere. This is also true for the water loading $5.3 \text{ molecules.nm}^{-2}$, for which the “Fe 2” is
 539 penta-coordinated (5c), thus its coordination sphere is not complete. Adding one water molecule

539 (coverage $6.4 \text{ molecules.nm}^{-2}$), now the coordination sphere of all Fe are complete, and the difference
 540 in the structures is that in the binuclear mode, the substituted water molecule is physisorbed at the
 541 surface. Now, the configurations are iso-energetic. This can be understood in the following way: the
 542 difference between mono- and bidentate being around 0.6 eV when no additional physically adsorbed
 543 water is present, the loss of energy due to the bidentate to monodentate transition may be compensated
 544 by the energy of one water molecule physisorbed at the surface.

545 From water loading $7.4 \text{ molecules.nm}^{-2}$ and above, the additional water molecules are
 546 physically sorbed at the surface. Now, the mononuclear configuration is more stable than the
 547 binuclear one. We note that additional water molecules tend to form a solvation-like structure around
 548 the COOH moiety. In the calculations, no spontaneous COOH deprotonation was observed. However,
 549 direct correspondence of this simple DFT modeling with a minimal number of water molecules to the
 550 multi-layer adsorption models of water on the goethite surface including the formation of “liquid-like
 551 water film” is difficult. The possibility of local solvation of COOH to COO^- by co-adsorbed water
 552 molecules will be studied in a next paper.
 553

Table 3: Most stable configurations obtained as a function of water loading for 0, 1, 2, 3, 4 and 5 water molecules (values of molecule/nm² are shown). The energy differences between bidentate (Bi) and monodentate (Mono) configurations ($\Delta E = \text{Mono} - \text{Bi}$) are given in eV.

554

a) 4.2 (Bi, 0,0)	b) 5.3 (Bi, 1,0)	c) 6.4 (Bi, 1,1)	d) 7.4 (Bi, 1,2)	e) 8.5 (Bi, 1,3)	f) 9.6 (Bi, 1,4)
					
	Fe 2 6c				
(Mono, 0,0)	(Mono, 1,0)	(Mono, 2,0)	(Mono,2,1)	(Mono, 2,2)	(Mono, 2,3)
					
Fe 2 5c Fe 2 4c	Fe 2 5c	Fe 2 6c			
$\Delta E = 0.61$	0.31	-0.04	-0.69	-0.29	-1.07

555

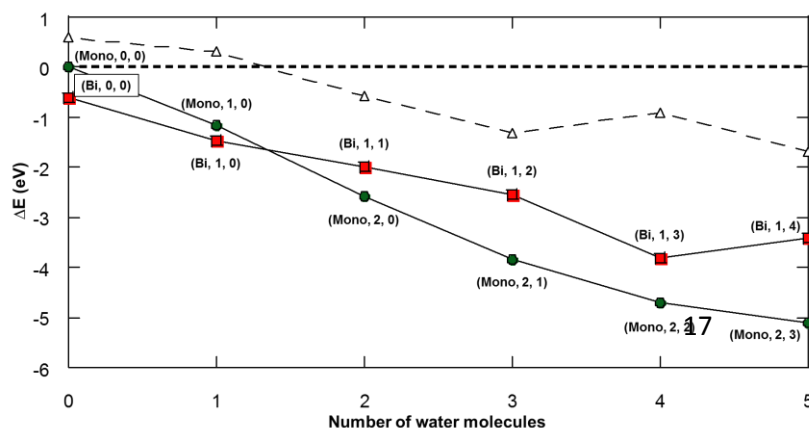


Figure 12: Adsorption energies of water on α -FeOOH (001) (with phthalate pre-adsorbed, as a function of the number of water molecules adsorbed for the monodentate (Mono: green circles) and the bidentate (Bi: red squares) adsorption modes. The dashed line represents the net difference between the energies of the two structures (values shown in Table 3).

556
557
558
559
560
561
562
563
564
565
566
567
568
569
570
571
572
573
574
575
576
577
578
579
580
581
582
583
584
585
586
587
588
589
590
591
592
593
594
595
596
597
598

Figure 12 shows the cumulative adsorption energies of water at the goethite surface, in the case of monodentate and bidentate adsorption. Both curves have a negative slope, indicating the stabilization of the system with water loading. The water adsorption energy for monodentate adsorption is higher than that for the bidentate adsorption at low water loading with 0 and 1 water molecules. This can be understood by the fact that at low water loading, water completes the Fe coordination sphere. For increasing water coverage, the monodentates become more stable and water molecules are physisorbed around the adsorbed phthalates, playing a secondary solvation role for the adsorbed phthalates.

These DFT calculations confirm the possibility of protonation of COO^- to COOH of phthalates adsorbed on the goethite surface with low water coverage. As a consequence, one of the carboxylate groups of the adsorbate can desorb and stay in a desorbed state and such a transformation is observed through the study of the different IR bands shown in the experimental part of this paper. The computational results obtained here are in good agreement with the experimental data with somewhat a better resolution of the phenomenon by adding water molecules one by one, which cannot be done with this experimental setup. The results provided by geometry optimization do not directly reproduce the spectroscopic trends but support the interpretation of experimental results.

Conclusion

By using IR spectroscopy combined with QCM and RH control system, we have been able to examine effects of a hydration/dehydration cycle on the speciation of phthalate ions adsorbed on goethite surface.

At low RH conditions, only small amounts of (ice-like) water are adsorbed on goethite surface and phthalates are considered to be adsorbed as bidentate by two carboxyl groups (COO^-) bound to the goethite surface. With increasing RH, water molecules are increasingly adsorbed and parts of carboxyl groups adsorbed on the goethite can be protonated to COOH by accepting protons from water molecules. The phthalates are still kept adsorbed by another carboxyl groups bound to the goethite surface. At high RHs, liquid-like water molecules are abundant at the goethite surface and some of protonated carboxyls can be deprotonated and solvated in water to form COO^- .

In order to test the above adsorption models based on experimental results, DFT simulations have been performed by adding 0 to 5 molecules of water to the goethite (001)/phthalate system. With low water coverage, water molecules participate in the coordination sphere of Fe with phthalates with bidentate more stable. At higher water coverage, monodentate becomes stable leading to partial desorption of phthalates. These DFT results support the above adsorption models.

These conclusions of this work can be a starting point for other environmentally and industrially relevant systems, such as the mobility of pollutants in geosphere during hydration/dehydration cycle, or for catalysts prepared by impregnation of dissolved precursors.

599 Acknowledgments

600

601 R.Botella has been supported by the International Research Fellowship of Japan Society for
602 the Promotion of Science (Postdoctoral Fellowships for Research in Japan (Summer Program)) at
603 Osaka University. This work was granted access to the HPC resources of CINES under the allocation
604 A0080802217 contributed by GENCI (Grand Equipement National de Calcul Intensif).

605

606

607 **Bibliography:**

608

- 609 [1] Kaiser, M.; Kleber, M.; Berhe, A., A. *Soil Biol. Biochem.* **2015**, 80, 324-340
610 [2] Bourikas, K.; Kordulic, C.; Lycourghiotis, A. *Catal. Rev.* **2006**, 48, 363-444
611 [3] Brinker, C., J. *MRS Bulletin* **2004**, 29, 631-640
612 [4] Clausen, L.; Fabricius, I. *J. Environ. Qual.* **2001**, 30, 858-869
613 [5] Nilsson, N.; Persson, P.; Lövgren, L.; Sjöberg, S. *Geochim. Cosmochim. Acta* **1996**, 60, 4385-4395
614 [6] McBride, M., B.; Wesselink, L., G. *Environ. Sci. Technol.* **1988**, 22, 703-708
615 [7] Maiti, E.; Öhman, L., O.; Nordin, J.; Sjöberg, S. *J. Colloid Interface Sci.* **1995**, 175, 230-238
616 [8] Wozniowski, T.; Malinowski, S. *J. Colloid Interface Sci.* **1980**, 77, 466-471
617 [9] Kishi, K.; Ikeda, S. *Surf. Sci.* **1980**, 5, 7-20
618 [10] Ramstetter, A.; Baerns, M. *J. Catal.* **1988**, 109, 303-313
619 [11] Kania, W.; Jurczyk, K.; Foltynowicz, Z. *Surf. Technol.* **1983**, 18, 349-358
620 [12] Le Bahers, T.; Pauporté, T.; Labat, F.; Lefèvre, G.; Ciofini, I. *Langmuir* **2011**, 27, 3442-3450
621 [13] G., Lefèvre, T., Preocanin, J., Lützenkirchen 2012. *Infrared Spectroscopy* Vol.1, T. Theophanides
622 (ed.), Intech, pp. 97-122
623 [14] Hwang, Y., S.; Liu, J.; Lenhart, J., J.; Hadad, C., M. *J. Colloid. Interface Sci.* **2007**, 307, 124-134
624 [15] Yang, Y.; Du, J.; Jing, C. *Colloids Surf. A* **2014**, 441, 504-509
625 [16] Hanna, K.; Martin, S.; Quilès, F.; Boily, J.-F. *Langmuir* **2014**, 30, 6800-6807
626 [17] Dobson, K., D.; McQuillan, A., J. *Spectrochim. Acta A* **1999**, 55, 1395-1405
627 [18] Rosenqvist, J.; Axe, K.; Sjöberg, S.; Persson, P. *Colloids Surf. A* **2003**, 220, 91-104
628 [19] Trout, C., C.; Kubicki, J., D. *J. Phys. Chem. A* **2004**, 108, 11580-11590
629 [20] Yesilbas, M.; Boily, J.-F. *J. Phys. Chem. Lett.* **2016**, 7, 2849-2855
630 [21] Asay, D., B.; Kim, S., H. *J. Phys. Chem. B* **2005**, 109, 16760-16763
631 [22] Mercury, L.; Nakashima, S. *Cheminform* **2006**, 37, 19-44
632 [23] Warring, S., L.; Beattie, D., A.; McQuillan, A., J. *Langmuir* **2016**, 32, 1568-1576
633 [24] Dol Hamid, R.; Miskelly, G., M.; Mat Hadzir, N.; Hanapi, N., S., M.; Swellund, P., J. *Appl.*
634 *Geochem.* **2018**, 91, 89-95
635 [25] Hug, S., J. *J. Colloid. Interface Sci.* **1997**, 188, 415-422
636 [26] Parfitt, R., L.; Smart, R., C. *Soil Sci. Am. J.* **1978**, 42, 48-50
637 [27] Persson, P.; Lövgren, L. *Geochim. Cosmochim. Acta* **1996**, 60, 2789-2799
638 [28] Kang, S.; Amarasiriwardena, D.; Xing, B. *Colloids Surf.* **2008**, 75, 4846-4856
639 [29] Kang, S.; Xing, B. *Langmuir* **2007**, 23, 7024-7031
640 [30] Rubasinghe, G.; Ogden, S.; Baltrusaitis, J.; Grassian, V. H. *J. Phys. Chem. A* **2013**, 117, 11316-
641 11327
642 [31] Prasad, B. *Environ. Sci.-Proc. Imp.* **2021**, 23, 389-399
643 [32] Das, M., T. ; Kumar, S., S.; Ghosh, P.; Shah, G.; Maylan, S., K.; Bajar, S.; Thakur, I., S.; Singh,
644 L. *J. Hazard. Mater.* **2021**, 409, 124496-
645 [33] Nakaya, Y.; Nakashima, S.; Otsuka, T. *Appl. Spectrosc.* **2021**, doi: 10.1177/0003702821991219
646 [34] Nakaya, Y.; Okada, K.; Ikuno, Y.; Nakashima, S. *e.-J. Surf. Sci. Nanotechnol.* **2018**, 16, 411-418
647 [35] Nakaya, Y.; Nakashima, S.; Otsuka, T. *Geochem. J.* **2019**, 53, 107-414
648 [36] Schwertmann, U., Cornell, R., M. 2000. *Iron oxides in the laboratory: preparation and*
649 *characterization* 2nd ed.: p. 188
650 [37] Otsuka, T.; Nakasima, S. *J. Miner. Petrol. Sci.* **2007**, 102, 302-305
651 [38] Nakaya, Y.; Nakashima, S.; Otsuka, T. *Appl. Spectrosc.* **2021**, DOI: 10.1177/0003702821991219
652 [39] Nakaya, Y.; Okada, K.; Ikuno, Y.; Nakashima, S. *e.-J. Surf. Sci. Nanotechnol.* **2018**, 16, 411-418

653 [40] Kudo, S.; Ogawa, H.; Yamakita, E.; Watanabe, S.; Suzuki, T.; Nakashima, S. *Appl. Spectrosc.*
654 **2017**, 71, 1621-1632

655 [41] Kudo, S. and Nakashima S., 2018. "Water Adsorption with Relative Humidity Changes for
656 Keratin and Collagen as Studied by Infrared (IR) Micro-spectroscopy". *Skin Res. Technol.* DOI:
657 10.1111/srt.12641

658 [42] Perdew, J. P.; Burke, K.; Ernzerhof, M. *Phys. Rev. Lett.* **1996**, 77, 3865–3868

659 [43] Kresse, G.; Hafner, J. *Phys. Rev. B* **1994**, 49, 14251–14269

660 [44] Kresse, G.; Joubert, D. *Phys. Rev. B* **1999**, 59, 1758–1775

661 [45] Kubicki, J. D.; Paul, K. W.; Sparks, D. L. *Geochem. Trans.* **2008**, 9, 4

662 [46] Otte K., Schmahl W. W., Pentcheva R. *Surf. Sci.*, 2012, 606, 1623-1632

663 [47] Alexandrov, V.; Rosso, K. M. *Phys. Chem. Chem. Phys.* **2015**, 17, 14518–14531

664 [48] Ohno, T.; Kubicki, J. D. *Phys. Chem. A* **2020**, 124, 3249–3260

665 [49] Paul, K. W.; Kubicki, J. D.; Sparks, D. L. *Eur. J. Soil Sci.* **2007**, 58 (4), 978–988

666 [50] Otte, K.; Schmahl, W. W.; Pentcheva, R. *J. Phys. Chem. C* **2013**, 117, 15571–15582

667 [51] Grimme, S. *J. Comput. Chem.* **2006**, 27, 1787-1799

668 [52] Cornell, R. M.; Schwertmann, U. 2003 *The iron oxides: structure, properties, reactions,*
669 *occurrences and uses*, 2nd ed.; Wiley-VCH: Weinheim,

670 [53] Nagano, T.; Nakashima, S.; Nakayama, S.; Osada, K.; Senoo, M. *Clay Clay Miner.* **1992**, 40, 600-
671 607

672 [54] Liu, H.; Chen, T.; Qing, C.; Xie, Q.; Frost, R., L. *Spectrochim. Acta A* **2013**, 116, 154-159

673 [55] Falk, M. *Spectrochim. Acta* **1984**, 1, 43-48

674 [56] Zhuang, H.; Lu, P.; Lim, S., P.; Lee, H.,P. *Langmuir* **2008**, 24, 8373-8378

675 [57] Ewing, G., E. *J. Phys. Chem. B* **2004**, 108, 15953-15961

676 [58] Colombo, L.; Volovsek, V.; LePostollec, M. *J. Raman Spectrosc.* **1984**, 15, 252-256

677 [59] Persson, P.; Nordin, J.; Rosenqvist, J.; Lövgren, L.; Öhman, L.-O.; Sjöberg, S. *J. Colloid.*
678 *Interface Sci.* **1998**, 206, 252-266

679 [60] Florio, G.; Zwier, T., S.; Myshakin, E., M.; Jordan, K., D.; Sibert, E., L. *J. Chem. Phys.* **2003**,
680 118, 1735-1746

681

682

683